Earth and Planetary Science Letters 443 (2016) 185–194

Contents lists available at ScienceDirect

Earth and Planetary Science Letters

www.elsevier.com/locate/epsl

Tidal dissipation in creeping ice and the thermal evolution of Europa

Christine McCarthy [a,*], Reid F. Cooper [b]

[a] Lamont-Doherty Earth Observatory, Columbia University, Palisades, NY, USA
[b] Department of Earth, Environmental and Planetary Sciences, Brown University, Providence, RI, USA

ARTICLE INFO

Article history:
Received 7 August 2015
Received in revised form 22 February 2016
Accepted 4 March 2016
Available online 25 March 2016
Editor: C. Sotin

Keywords:
ice
attenuation
dislocations
icy satellites
microstructure
anelasticity

ABSTRACT

The thermal and mechanical evolution of Europa and comparable icy satellites—the physics behind creating and sustaining a subsurface water ocean—depends almost entirely on the mechanical dissipation of tidal energy in ice to produce heat, the mechanism(s) of which remain poorly understood. In deformation experiments, we combine steady–state creep and low-frequency, small-strain periodic loading, similar conditions in which tectonics and tidal flexing are occurring simultaneously. The data reveal that the relevant, power-law attenuation in ice (i) is non-linear, depending on strain amplitude, (ii) is independent of grain size, and (iii) exceeds in absorption the prediction of the Maxwell solid model by an order of magnitude. The Maxwell solid model is widely used to model the dynamics of planetary ice shells, so this discrepancy is important. The prevalent understanding of damping in the geophysical context is that it is controlled by chemical diffusion on grain boundaries, which renders attenuation strongly dependent on grain size. In sharp contrast, our results indicate instead the importance of intracrystalline dislocations and their spatial interactions as the critical structural variable affecting dissipation. These dislocation structures are controlled by stress and realized by accumulated plastic strain. Thus, tectonics and attenuation are coupled, which, beyond the icy satellite/subsurface ocean problem, has implications also for understanding the attenuation of seismic waves in deforming regions of the Earth's upper mantle.

1. Introduction

Although water ice is one of the most common substances in the solar system, it is also one of the most enigmatic, with much remaining unknown about its viscoelastic properties. To interpret surface features of icy satellites and to model thermal evolution via tidal dissipation, a thorough understanding of the rheological properties of ice and ice-rich mixtures at planetary conditions is needed. Without such experimental data, processes on icy satellites typically have been modeled using a simple Maxwell solid or a steady–state rheology (e.g., Ojakangas and Stevenson, 1989). However, the disparity between predicted behavior using Maxwell's model and observed behavior from recent satellite-based measurements (e.g., geysers and tectonics) demonstrates the need to refine such models to include the spectrum of mechanical response from elastic to anelastic to viscous (Shoji et al., 2013). To account for significant heat generated by mechanical dissipation of tidal forces, a transient, anelastic response is required. Since microstructure influences transient/anelastic properties and steady–state behavior establishes and sustains microstructure, the overlap of transient and steady–state behavior is important for tidal processes. Further, the ability to extrapolate laboratory data to planetary dynamics requires understanding of the physics of dissipation and how it scales with frequency, grain size, and temperature, as well as with stress and accumulated strain.

On Europa, the global stress field within the icy shell includes a diurnal component with a frequency $f = 3 \times 10^{-6}$ Hz from periodic tidal flexing with a strain amplitude of $\sim 10^{-5}$ (Tobie et al., 2003). Additionally the presence of the liquid ocean decouples the shell, resulting in a significantly larger component of tidal stress from reorientation of the tidal bulge relative to the parent body's direction, called nonsynchronous rotation, which has a larger strain amplitude and much larger period ($\sim 10^{13}$ s) (Greenberg et al., 1998). In addition to these two periodic stresses, it is posited that convective overturn can occur within an icy shell creating a stress on the order of tens to hundreds of kPa (Pappalardo et al., 1998).

Here we describe and interpret the results from a series of experiments that measure the anelastic response of polycrystalline ice simultaneously experiencing a cyclic load and a constant steady–state load at realistic stress/strain amplitudes and at frequencies approaching those of satellite tides. The tests highlight the fact that different mechanisms act at different timescales: the

* Corresponding author.
E-mail address: mccarthy@ldeo.columbia.edu (C. McCarthy).

http://dx.doi.org/10.1016/j.epsl.2016.03.006
0012-821X/

mechanism rate-limiting high-strain creep need not be the same as that providing the relaxation of a small periodic perturbation. The beauty of attenuation is that it can be used as *mechanical spectroscopy* to see the mechanisms (via small disturbances) shrouded by the steady–state behavior.

2. Experimental method

In this study deformation experiments were conducted on polycrystalline ice samples. We used three different methods of sample preparation in order to obtain specimens with four distinct grain sizes: (1) coarse (C: $d \sim 300$ μm); (2) medium (M: $d \sim 150$ μm); (3) fine (F: $d \sim 20$ μm); and (4) very fine (VF: $d \sim 8$ μm). Those methods were: bulk solidification from seeded water to create C samples (McCarthy et al., 2007); nebulization of water with flash freezing followed by sieving to desired particle size and "hot"-pressing to create M and F samples (Goldsby and Kohlstedt, 1997); and ice-II to ice-I phase transformation via a pressure release protocol to create VF samples (Durham et al., 2001). The details of each fabrication method can be found in Appendix A.1. Sample characterization was conducted using a scanning electron microscope (SEM) fitted with a cryogenic preparation station. Secondary electron images (SEI) were taken of fresh fracture surfaces while remaining under vacuum with $T < 100$ K and a low accelerating voltage of 2 kV (Fig. 1). Sublimation rates in the SEM are known to be higher at grain boundaries, ostensibly etching the samples (Cullen and Baker, 2001). Grain size was measured for each of the VF, F, and C samples using the line intercept method on SEM images, with a correction factor of 1.5 (Gifkins, 1970). A total of 7 transects and 53 grains were counted from three VF sample images; 24 transects and 252 grains were counted from seven F sample images; and 5 transects and 28 grains were counted from one C sample image. The grain size errors listed parenthetically in Table 1 represent the standard deviation from the mean of these counts. Several samples were examined prior to deformation and after deformation and no discernable grain growth occurred during mechanical testing.

Using a commercial servomechanical-actuator testing apparatus that was modified for cryogenic conditions, samples were subjected to a sinusoidally time-varying compressive stress superposed upon a constant, median applied compressive stress. The resulting strain—a steady–state creep strain plus a periodic anelastic strain—was measured with a gravity-fed extensometer that, by specifications, could resolve differential strains of $\varepsilon = 5 \times 10^{-7}$; thermal noise limited the strain resolution to 5×10^{-6}. Complex modulus and attenuation Q^{-1} are measured from the amplitude ratio and the tangent of phase delay δ, respectively, of the peak stress σ and peak strain ε. (A detailed description of the apparatus and data analyses are provided in Appendix A.) In this study the tests employed uniaxial loading so that the properties measured were Young's modulus E and attenuation Q_E^{-1}. In most cases, the median applied stress was $\sigma_m = 1$ MPa (Table 1). For this median stress, and the temperatures and grain sizes of the majority of these samples, the steady–state flow was accomplished by grain boundary sliding that is strain-accommodated by basal dislocation slip (Goldsby and Kohlstedt, 2001), the mechanism thought to be most applicable to tectonic processes in the geophysical ice-shell problem (Barr and Showman, 2009). In the case of the coarsest-grain-sized specimens in this study, deformation conditions were instead consistent with dislocation creep. The range of applied stress sinusoids studied was $\sigma_0 = 0.05$–0.28 MPa (cyclic strain amplitude $\varepsilon_0 \approx 5 \times 10^{-6}$–$3 \times 10^{-5}$), with 0.167 ± 0.006 MPa (1.7×10^{-5}) being the amplitude used for most tests (and 0.16 MPa the value used for analyses). Testing was conducted in the temperature range $200 \leq T(\mathrm{K}) \leq 260$ and over the frequency range 10^{-4}–10^{-1} Hz. Error was determined by performing multiple tests (between three and five, depending on frequency) and plotting the mean value and absolute variation thereof.

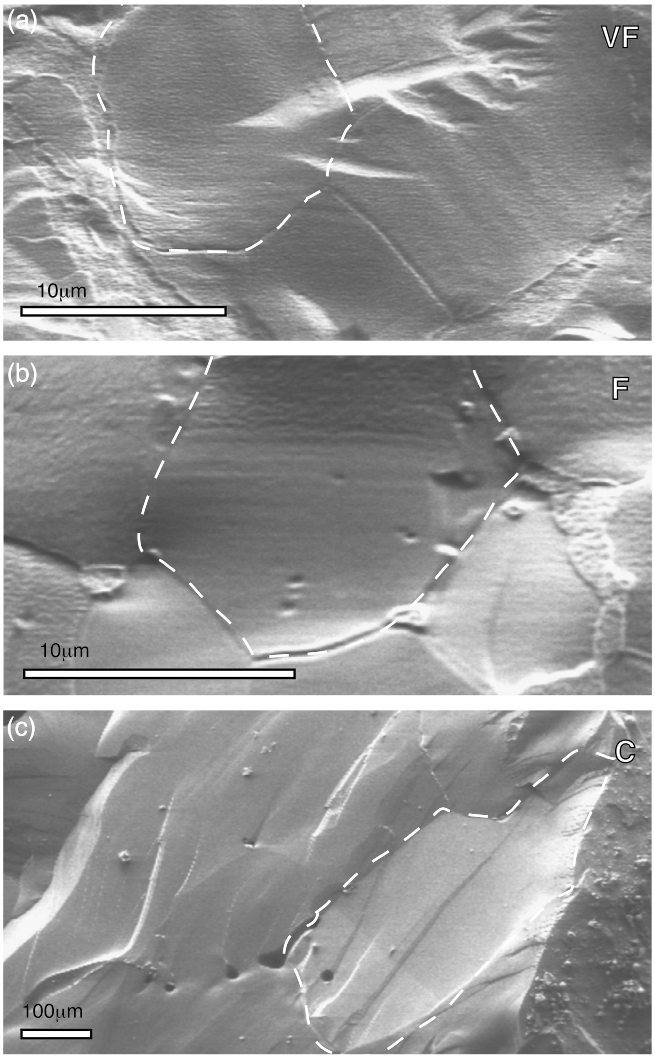

Fig. 1. SEM/SEI images of water ice-I made via three different fabrication techniques: (a) very fine-grained VF (8.4 ± 1.8 μm) made by pressure release method which results in subdivision of originally larger, spherical grains; (b) fine-grained F (19.9 ± 3.0 μm) prepared by droplet solidification, in which triple junctions and pronounced grain boundary troughs can be seen; and (c) coarse-grained C (300 ± 60 μm) grown slowly by bulk solidification in test tubes. A fourth grain size, medium-grained M (<180 μm) was also fabricated using the droplet solidification method (but a larger sieve), but was not imaged. Grain size for specimens M is estimated from the sieve size. A dashed white line in each figure roughly outlines a single grain.

3. Experimental results

The steady–state effective viscosities demonstrated by our specimens are consistent with those from previous experimental studies on similar polycrystalline specimens of ice-I (e.g., Goldsby and Kohlstedt, 2001). A typical creep curve from initial loading (prior to the periodic loading) is provided in the Appendix (Fig. A.2(a)). Fig. 2 presents the results of linearity tests, which were confined to the F (~20 μm) specimens and run at $f = 0.01$ Hz. The median differential stress for all tests was $\sigma_m = 1$ MPa. The material demonstrates a modest strain-amplitude dependence of attenuation, $Q_E^{-1} \propto \varepsilon_0^{0.39}$, with the response insensitive to temperature, to first order.

Attenuation and Young's modulus data for the fine-grained (F) samples as a function of testing temperature are presented in Fig. 3. The data display clear temperature dependence, with, at

Table 1
Experimental conditions for dynamic testing and Maxwell frequency f_M used for scaling in Fig. 5.

Grain size (μm)	Grain size designation	T (K)	Median stress σ_m (MPa)	Stress amplitude σ_0 (MPa)	Frequency range f (Hz)	f_M (s^{-1})[a] ε/η_{ss}
8.4 (1.8)	VF	220	1.0	0.168	2.5×10^{-4}–2.5×10^{-2}	2.19×10^{-5}
8.4 (1.8)	VF	240	1.0	0.167	10^{-3}–5×10^{-2}	3.08×10^{-4}
8.4 (1.8)	VF	260	0.78	0.168	2.5×10^{-4}–10^{-2}	1.75×10^{-3}
19.9(3)	F	200	1.0	0.171	7.5×10^{-4}–10^{-1}	9.27×10^{-7}
19.9(3)	F	220	0.96	0.168	2.5×10^{-4}–5×10^{-2}	2.02×10^{-5}
19.9(3)	F	220	1.07	0.168	10^{-1}	2.52×10^{-5}
19.9(3)	F	240	0.87	0.172	10^{-3}–2.5×10^{-1}	2.33×10^{-4}
19.9(3)	F	240	0.96	0.166	10^{-4}	2.89×10^{-4}
19.9(3)	F	240	1.04	0.173	2.5×10^{-4}–7.5×10^{-3}	3.33×10^{-4}
19.9(3)	F	250	1.0	0.169	7.5×10^{-3}–7.5×10^{-2}	9.57×10^{-4}
19.9(3)	F	260	0.84	0.168	10^{-3}–5×10^{-2}	2.02×10^{-3}
100–180	M	240	1.0	0.165	5×10^{-4}–7.5×10^{-2}	3.08×10^{-4}
100–180	M	260	1.0	0.165	10^{-2}–10^{-1}	2.87×10^{-3}
300(60)	C	240	1.0	0.165	10^{-3}–7.5×10^{-3}	3.08×10^{-4}
300(60)	C	260	1.27	0.163	10^{-3}–7.5×10^{-3}	4.63×10^{-3}
300(60)	C	260	1.44	0.162	7.5×10^{-3}–10^{-2}	5.96×10^{-3}
300(60)	C	260	1.69	0.162	5×10^{-4}–5×10^{-3}	8.27×10^{-3}

[a] η_{ss} is the diffusion creep viscosity estimated using Goldsby and Kohlstedt (2001) at the given T and a subgrain size calculated from Raj and Pharr (1986) at σ_m.

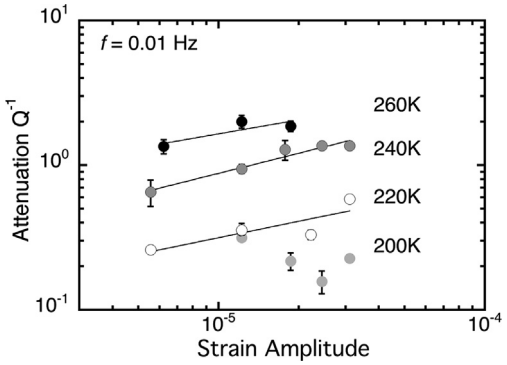

Fig. 2. Measured attenuation vs. strain amplitude (the latter calculated using the known applied stress normalized by the temperature dependent unrelaxed Young's modulus). Data represent fine grain samples (F) tested at $f = 0.01$ Hz. Where error bars are not apparent, it is because they are less than the size of the symbols. The slope of the 260 K line is 0.32, the slope of the 240 K line is 0.46 and the slope of the 220 K line is 0.38. The 200 K data show considerable scatter.

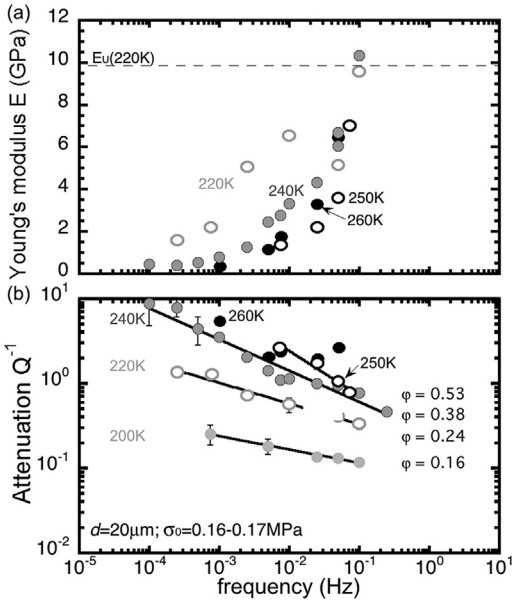

Fig. 3. Measured (a) modulus dispersion and (b) attenuation, as functions of frequency and temperature for fine grain-sized samples (F; ~20 μm) made by droplet solidification/hot-pressing. The reciprocating stress amplitude σ_0 was constant in all the tests, but the median stress σ_m varied from 0.83 MPa (260 K data) to 1.04 MPa (see Table 1).

fixed frequency, decreasing effective modulus and increasing attenuation with increasing temperature. The form of the attenuation spectra (Fig. 3(b)) is a modest power-law relationship with frequency, $Q_E^{-1} \propto f^{-\varphi}$, where φ increases with temperature from ~0.16 at 200 K to ~0.5 at 250 K. (Data from 260 K are too scattered to fit responsibly with a line.) Significant and almost total relaxation of the modulus from its high-frequency (i.e., unrelaxed or anharmonic) value E_U is observed (Fig. 3(a)).

Determination of activation enthalpy (E_A) for the anelastic response is problematic: the variation of φ for different temperature conditions affects significantly the characterization. Activation enthalpy is discerned not by variation of Q_E^{-1} with temperature but, rather, by the shift in frequency for a specific attenuation response—consistent with Boltzmann statistics (Nowick and Berry, 1972 (p. 458); Cooper, 2002). Working through Figs. 3 and 4 at $Q_E^{-1} = 1$, for example, reveals a range for E_A of 25–85 kJ mol^{-1} ($E_A = 58 \pm 25$ kJ mol^{-1}); analyses for other values of Q_E^{-1} confirm the spread.

A comparison of attenuation spectra as a function of grain size and temperature is shown in Fig. 4. The data demonstrate clear temperature dependence with a consistent φ value amongst samples at each temperature. In contrast, there is very little—to first order, no—dependence of attenuation on grain size, with the exception that F samples are slightly more attenuating than other samples.

4. Discussion

The results from our study display an apparent dichotomy in the mechanical behavior. The $Q_E^{-1} \propto f^{-\varphi}$ power-law response is associated with strictly Newtonian (linear viscous) behavior, which is very sensitive to grain size, whereas the observed strain amplitude dependence is associated with non-Newtonian (non-linear) behavior; further, the attenuation response is independent of grain size, to first order. The seemingly contradictory nature must be reconciled before extrapolation can occur. A first step is to differentiate between the mechanism dominating the viscous response and the mechanism(s) employed by the system to dissipate energy from a small-in-magnitude, limited-in-duration pulse. These mechanisms need not be the same. The steady state response creates and sets the microstructure that the anelastic perturbation "samples". Here we will take the individual elements of the response, compare the data to previous studies, and by doing so, parse out

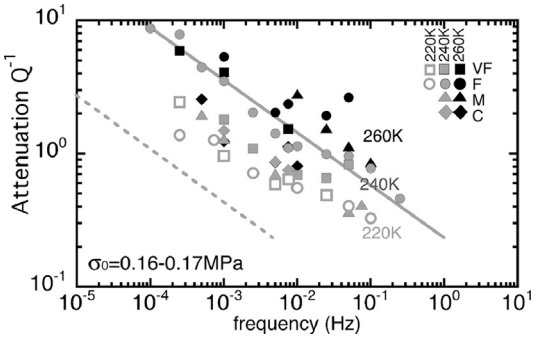

Fig. 4. Measured attenuation vs. frequency as a function of grain size at 220 K, 240 K, and 260 K. The solid gray line is a simple approximation of the F (∼20 μm) data at 240 K (gray circles). The dashed line is an extrapolation of this data to predict the response of C samples (∼300 μm) based on an inverse cube of grain size relationship for the viscosity term of the Maxwell frequency, which is the prevailing theory for the grain size dependence of attenuation in this frequency range. The predicted attenuation is significantly lower than that measured for any of the grain sizes at this temperature, demonstrating that in our study attenuation is independent of grain size, to first order.

an understanding of the attenuation response in an actively deforming material.

4.1. Previous studies: diffusionally accommodated GBS

Previous studies have determined a universal anelastic response for polycrystalline materials deforming by Newtonian (diffusional) creep (e.g., Gribb and Cooper, 1998; Tan et al., 2001; Jackson et al., 2002; Sundberg and Cooper, 2010). By keeping deviatoric stresses low and grain size small, these studies ensured that no lattice dislocations were nucleated during testing. Thus, the "attenuation band" behavior, that is, the modest power-law frequency dependence in Fig. 5, is attributed to "diffusionally accommodated grain boundary sliding" whereby a deviatoric stress creates high stress concentrations at grain triple junctions that are alleviated through chemical diffusion at length scales of the grain size or larger (e.g., Gribb and Cooper, 1998; Raj and Ashby, 1971; Raj, 1975; Morris and Jackson, 2009). The relaxation time τ is not that associated with exponential decay, i.e., as represented by the standard anelastic solid, but rather that associated with deviatoric-stress-effected chemical diffusion:

$$\tau = \frac{3\sqrt{3}(1-\nu^2)d^3kT}{2\pi^3 E_U D_b \zeta \Omega} \tag{1}$$

where ν is Poison's ratio, k is Boltzmann's constant, D_b is the grain-boundary diffusion coefficient of the rate-limiting ionic species, ζ is the grain-boundary thickness and Ω is molecular volume (Raj, 1975). In that case, the physics of this relaxation are identical to that of steady–state creep dominated by grain-boundary diffusion; as a consequence, the relaxation time can be directly calculated from the unrelaxed modulus and the steady–state, diffusional (Newtonian) viscosity (η_{ss}), as (Gribb and Cooper, 1998)

$$\tau \cong \frac{10\eta_{ss}}{E_U} \tag{2}$$

Equations (1) and (2) provide the "license" for normalizing the power-law, high-temperature-background attenuation spectra by the Maxwell frequency, $f_M \equiv 1/\tau_M = M_U/\eta_{ss}$, where M_U is the unrelaxed modulus for the applicable mode of testing (McCarthy et al., 2011; Morris and Jackson, 2009). For polycrystalline materials characterized by a Newtonian steady–state viscosity, such normalization results in a master curve on the log Q^{-1} v. log (f/f_M) plot and a relaxation time τ that is highly sensitive to grain size: $\tau \propto d^3$. The compiled data are compared to a frequency-transformed Andrade creep function, which is described more fully in Appendix C. The similitude demonstrated by this normalization is presented in Fig. 5, which includes numerous datasets for polycrystalline olivine-dominated specimens as well as for polycrystalline organic borneol. The efficacy of the master curve method in identifying the diffusionally-based mechanism provides an excellent framework then to analyze other materials that are not deforming by Newtonian (diffusional) creep. In the similarities and differences we can determine the relative importance of other dissipation mechanisms, namely dislocations.

4.2. The importance of subgrains

Lattice dislocations, because of their high intrinsic energy, arrange themselves in arrays that constitute subgrain boundaries (e.g., Sutton and Balluffi, 1995 (Ch. 2)), the spacing distribution of which depends primarily on the deviatoric stress; temperature only enters consideration with regard to its effect on the unrelaxed shear modulus (Twiss, 1977; Raj and Pharr, 1986). The array of subgrain boundaries, nominally in a log-normal distribution, facilitates dislocation plasticity in that (a) the distribution of subgrains is self-similar to that for "free" (i.e., mobile) dislocations (Weertman and Weertman, 1983; Stone et al., 2004) and (b) diffusional creep of the subgrains is an integral process in dislocation-effected plasticity, one that acts in kinetic parallel (i.e., independently) with dislocation glide (Stone et al., 2004; Stone, 1991). Thus, for materials with a dislocation/subgrain structure set by a dislocation rheology, as is the case for the specimens in this study, one might replace the grain size in Eq. (1) with the mean subgrain size.

We can illustrate the effect of subgrains on attenuation by examining Fig. 5, in which we included attenuation data as a function of normalized frequency for a forsterite single crystal that was previously deformed to steady state in the dislocation creep regime (Gueguen et al., 1989). Application of these data to the figure was done using the observed relationship between applied stress and subgrain size from numerous datasets compiled by Raj and Pharr (1986), in which $d_{SG} = K\mu b/\sigma_m$, where μ is shear modulus, b is the Burgers vector, and constant $K = 23$. The 1600 °C/20 MPa steady–state creep conditions equate to a mean subgrain size in the forsterite crystal of $d_{SG} = 33$ μm. The normalization used the 1200 °C diffusional creep viscosity measured for forsterite (Thompson et al., 2011), with extrapolations using a grain-size exponent of 3 [i.e., $\eta_{ss} \propto d^3$ (Coble, 1963; Frost and Ashby, 1982)] and a thermal activation energy of 500 kJ mol^{-1} (cf. Hiraga et al., 2010). Using these parameters, and the temperature-dependent unrelaxed modulus (Frost and Ashby, 1982), a 33 μm "grain size" produces $f_M = 9.3 \times 10^{-8}$ s^{-1} for the 1200 °C attenuation data and 1.2×10^{-5} s^{-1} for the 1400 °C data. The normalized deformed-single-crystal data collapse nicely onto the attenuation master curve, although much of the data exist in a f/f_M range of higher frequency than the others. Similitude with the other studies indicates the same mechanism is acting; our analysis shows that in the deformed single crystal case, it is diffusion at the subgrain boundaries responsible for the response. The critical issue in applying the model in Eq. (1) is identifying the characteristic length for chemical diffusion. In Newtonian aggregates having a steady–state diffusional rheology, that characteristic length is the grain size. As will be explored further below, in materials deforming in steady state via a dislocation rheology, the characteristic diffusion length is the subgrain size.

The ice specimens we studied are creeping at steady state in the GBS regime or near its transition to dislocation creep. Significant amounts of the plastic strain at steady state are being accomplished by the motion of dislocations. Consequently, steady–

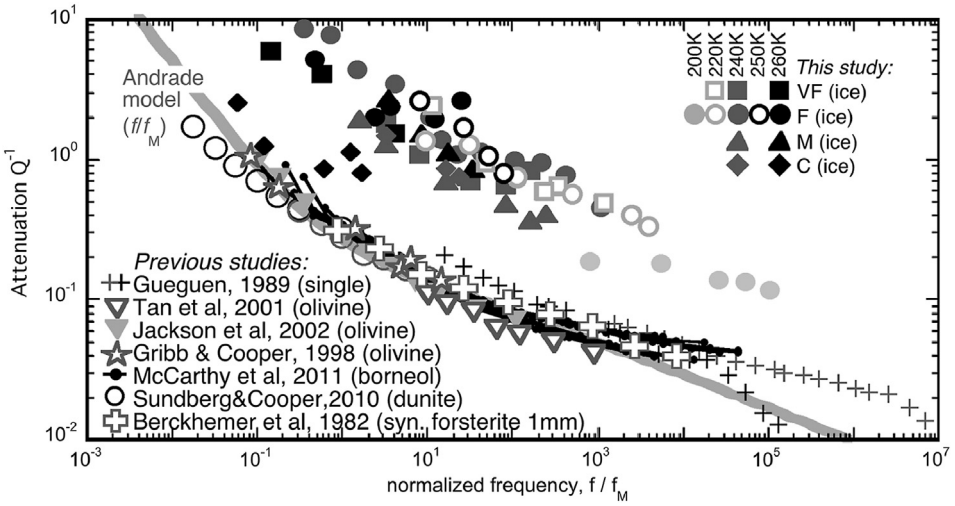

Fig. 5. Measured Q^{-1} for polycrystalline materials at various temperatures and grain sizes. All data have been normalized by the Maxwell frequency ($f_M = M_U/\eta_{ss}$) where η_{ss} is the steady-state diffusion creep viscosity. Data for olivine are from Gueguen et al. (1989) (1200 and 1400 °C; pre-deformed forsterite single crystal), Gribb and Cooper (1998) (1200 and 1250 °C; $d = 3$ μm), Jackson et al. (2002) (1200 °C; $d = 2.9$ μm), Tan et al. (2001) (1200 °C; $d = 23.6$ μm), Sundberg and Cooper (2010) (1200 and 1300 °C; $d = 5$ μm), and Berckhemer et al. (1982) (1400 °C; $d = 1$ mm synthetic forsterite); data for borneol is from McCarthy et al. (2011) (20–50 °C; $d = 3$–22 μm). In ice data from this study, η_{ss} is estimated diffusion creep viscosity from Goldsby and Kohlstedt (2001) assuming a grain size consistent with the stress-dependent subgrain size and temperature dependent moduli. The gray line is the Andrade model using η_{ss} estimate assuming diffusion creep in ice (1.4×10^{16} Pa s), a Young's modulus of 9 GPa, and best fit parameters for β and ψ (4.5×10^{-12} and 0.25, respectively; cf. SI) and normalized by the Maxwell frequency.

state flow in these regimes is consistent with a subgrain structure, which has been recently characterized both by careful experimental ice-rheology study (Hamann et al., 2007) as well as by observational work of deforming ice from Antarctic drill cores (Weikusat et al., 2009). Comparison of the experimental observations of subgrain distribution in Hamann et al. (2007) with the relationship between subgrain size and stress prediction of Raj and Pharr (1986) demonstrate a direct correlation. The relationship between stress and subgrain size yields a value of $d_{SG} \approx 37$ μm for ice deforming at steady state at 1 MPa. Combined with the temperature-dependent unrelaxed moduli for ice (Gammon et al., 1983) and a parameterization for diffusional creep of ice (Goldsby and Kohlstedt, 2001; cf. Frost and Ashby, 1982), all of the attenuation data collected in this study have been normalized based on mean subgrain size and plotted with the other attenuation data in Fig. 5. Two points are obvious: (1) with the exception of the highest-temperature (260 K) data for the coarsest-grain-sized material, which exhibit significant experimental scatter, the data for the experiments take the same form as the high-temperature-background "master curve"; (2) the attenuation of the deforming ice aggregates in our experiments is approximately an order of magnitude greater at a given frequency than that of the materials in the master curve. (Note that, although there is no theoretically justified reason to do so, normalizing instead with a GBS or dislocation viscosity also yields a curve significantly offset from the master curve of the other studies. Normalizing instead with the diffusion viscosity for the actual average grain size would shift the VF samples ~1 order of magnitude closer to the master curve, the F samples would be nearly the same, but the M and C samples would shift ~2 orders of magnitude farther to the right.)

4.3. Dissipation by lattice dislocations

The rock physics/materials science understanding of dislocation damping is evolving. Non-linear results such as ours have historically been treated with the dislocation-glide-damping model of Granato and Lücke (1956a, 1956b); cf. Minster and Anderson (1981), Karato and Spetzler (1990), Farla et al. (2012). Their model assumes dislocations pinned by other dislocations and/or by impurities, producing either frequency-dependent attenuation via motion constrained by the pinning—essentially the vibration of dislocations—or frequency-independent attenuation based on dislocation glide after breaking away from pinning. A statistical spatial distribution of pinning points is required to produce a distribution of compliances, but reasonable assumptions for impurities, etc., cannot replicate the form or frequency of our data: the processes articulated by Granato and Lücke, for reasonable assumptions of stress and temperature (normalized to modulus and melting temperature, respectively), apply to frequencies higher than the ones studied in our experiments and, additionally, produce $\varphi \geq 1$ for the frequency-sensitive attenuation response in material that includes an exponential distribution of dislocation pinning lengths. Clearly, the model cannot explain the present results.

A way forward in understanding the measured attenuation response takes advantage of recent experimental characterizations of dislocation plasticity in ice. Steady-state flow in ice has been demonstrated to involve intermittent emissions and motions of collections of dislocations—dislocation "bursts"—that have been characterized by acoustic emissions (Miguel et al., 2001; Richeton et al., 2005; Weiss et al., 2015). These studies reveal self-organized, critical (SOC) behavior in deforming ice, identified by an inverse power law relationship between the energy magnitude of a dislocation burst and the frequency of bursts at that magnitude. Such a mechanical result is inconsistent with the textbook understanding of crystalline plasticity based upon the behavior of the "average" dislocation (e.g., Frost and Ashby, 1982). The result, however, is certainly consonant with the dislocation substructure in steady-state creep being statistical in nature and self-similar, as introduced earlier (e.g., Stone et al., 2004; Zaiser and Hähner, 1999). Further, the statistical, SOC nature of plasticity is consistent with Stone's (1991) model for dislocation creep, which is predicated on the equation-of-state approach to plasticity championed by Hart (1970) and demonstrated to hold for all classes of crystalline solids [metallic (e.g., Hart and Solomon, 1973), ionic (e.g., Stone et al., 2004; Lerner et al., 1979) and covalent (e.g., Chiang and Kohlstedt, 1985)]. The model partitions strain between diffusional creep of subgrains and temperature-insensitive (athermal) glide, depending on the exact size of a given subgrain relative to the stress. In thinking about attenuation, perturbations in stress, those small in magnitude and of limited temporal extent

relative to the stress sustaining the steady–state flow, merely "tickle" this self-similar substructure without prompting its adjustment. The predicted anelastic response is linear, i.e., that associated with diffusional transients with the subgrain size defining the characteristic length scale, as introduced above—hence the linear anelastic response of the dislocation-creep-deformed forsterite crystal described earlier and presented in Fig. 5 (Gueguen et al., 1989). There is, however, a threshold stress perturbation where mobile dislocations are nucleated/emitted from grain and subgrain boundaries (cf. Gifkins, 1976), and within the context of Stone's model (1991), SOC behavior in plasticity, then, can be understood as setting a stress- and temperature-sensitive probability for achieving the threshold and so the emission of dislocations that can glide across one or several subgrains or even the entire specimen (Puthoff, 2005).

We can scrutinize Fig. 5 to calculate the energy dissipation by dislocation motion alone. Glide of dislocations is "pure" dissipation: plasticity being a constant-volume process, elastic energy stored in the bonds of a stressed material is converted entirely into heat by the glide motion. Consider, as an example, a datum from the center of our experimental set—a fine-grain-size (F) ice specimen tested at 240 K with $\sigma = \sigma_m \pm \sigma_0 = 1 \pm 0.16$ MPa. The material demonstrates a $Q_E^{-1} = 2$ at $f = 3 \times 10^{-3}$ Hz and a measured $E = 1.3$ GPa (Fig. 3; this datum can be located at $Q_E^{-1} = 2$ and $f/f_M \approx 10^1$ Hz in Fig. 5); thus, $\varepsilon_0 \cong 9 \times 10^{-4}$ and the storage modulus ($E' = E \cos\delta$) is 0.58 GPa. One can compare this to the master curve for the polycrystalline data, where the attenuation is an order-of magnitude lower, i.e., $Q_E^{-1} = 0.2$. For this master-curve value of Q_E^{-1}, the storage modulus is estimated as $0.97E_U$ (from a Lissajous figure, e.g., Lakes, 1999 (p. 68)), which at 240 K is 9.2 GPa. For a half-cycle of loading, with this modulus and $\sigma_0 = 0.16$ MPa, the stored elastic energy is $W_s = 115$ J m^{-3}; thus, following the definition of Q^{-1} as the energy dissipated per radian, i.e.,

$$Q^{-1} \equiv \frac{1}{2\pi}\left(\frac{W_d}{W_s}\right) \tag{3}$$

where W_d is the dissipated energy (e.g., Nowick and Berry, 1972 (p. 22), Lakes, 1999 (p. 76)), the dissipated energy for $Q_E^{-1} = 0.2$ is $W_d = 144$ J m^{-3}. The additional dissipated energy of the actual specimen, with a $Q_E^{-1} = 2$, then, is $\Delta W_d = 1296$ J m^{-3} and represents a plastic strain of $\sim 8 \times 10^{-4}$.

The self-similar microstructural state of the ice in our experiments associated with the subgrain-size distribution is "set" by the mean stress, σ_m, which for most of our experiments is 1.0 MPa. A distribution of subgrain sizes in a self-similar structure must relate to a distribution of mobile dislocations, which in turn can be characterized by a mean dislocation density, ρ_d (Stone et al., 2004). Plastic strain (and energy dissipation) is given by the product of the dislocation density times the magnitude of the Burgers vector (b [$= 4.52 \times 10^{-10}$ m for basal dislocations in ice]) times the average distance traveled by a dislocation (x), i.e., $\varepsilon = \rho_d b x$. Application of the strain-energy piezometer, here $\rho_d = (\sigma_m/[3\mu_U b])^2$ (e.g., Weathers et al., 1979), at 240 K and with $\sigma_m = 1$ MPa gives $\rho_d = 4.2 \times 10^{10}$ m^{-2}. Thus, the plastic strain of 8×10^{-4} can be achieved by the ρ_d mobile dislocations gliding by 40 μm, which is approximately the same as the subgrain size.

The result is a satisfying one: a release and glide of the average density of dislocations across the average subgrain size characterizes the additional energy dissipated over a condition where the modulus is only modestly relaxed. Use of average (mean) quantities is justified in the same spirit as that involved in, e.g., other dissipative, power-law systems (e.g., Weertman and Weertman, 1983; Stone et al., 2004) or in the description of bulk thermodynamic parameters such as system enthalpy. Of course, the same calculation done with data from other frequencies would not be as easily interpreted physically: at lower frequencies, an order of magnitude additional dissipation over the master curve represents significantly more additional dislocation glide while the opposite is true at higher frequency.

The first-order lack of dependence of the attenuation response on grain size provokes additional comment. Given that we have explored a grain size range of approximately two orders of magnitude, and that distinctly finer-grain-size material (VF; ~8 μm) shows the same attenuation at lower frequency, an attenuation, too, that matches that of our coarse (C; ~300 μm) material, informs our claim of grain-size independence. One ramification of this argument is that the subgrain size that we used to normalize our attenuation data in Fig. 5—37 μm—is coarser than our finest grain size material (VF). Analysis of the relative strain energy densities of dislocations, subgrain boundaries and grain boundaries support the idea that dislocation networks can have scales exceeding the grain size (e.g., Lubarda et al., 1993); further, plastic flow effected by dislocations can occur in a kinetic regime that doesn't "feel" the grain boundaries (e.g., Crossman and Ashby, 1975). It remains interesting, however, that the one specimen type having a subgrain size and grain size approximately equal demonstrates the greatest attenuation—albeit not by much, but well within experimental resolution—in these experiments, suggesting as additive the grain-boundary sliding/subgrain boundary sliding/dislocation emission effects. The additive kinetic responses combined with the fractal distribution of subgrain sizes associated with steady–state creep address, in part, the breadth of activation energies seen in our experiments. The range of values for E_A (58 ± 25 kJ mol^{-1} at $Q_E^{-1} = 1$) is consistent with dislocation and diffusional mechanisms both being involved in the anelastic response (e.g., Goldsby and Kohlstedt, 2001; cf. Cole and Durell, 2001).

4.4. Application to geophysical contexts

The findings of this study have implications for both seismic attenuation in the Earth's upper mantle and tidal dissipation on icy satellites. Regions of the upper mantle that display seismic anisotropy are interpreted as being deformed (either actively or in the past) via dislocation creep in response to the tectonic stress. Consistent with the results from a previous study on pre-deformed olivine samples (Farla et al., 2012), our study suggests that seismic attenuation may be enhanced by deformation-induced microstructure. However, additional testing, particularly at normalized frequencies that should be those of the seismic band are needed to accurately scale and predict the magnitude of the effect. The frequencies of tidal loading of some icy satellites, however, are well within the normalized range shown in Fig. 5 (depending on the size and period of the moon). In these cases, direct extrapolation can be performed by determining the stress associated with solid-state convection in the ice shell and calculating from this stress and the mean temperature a characteristic subgrain size. As the temperatures and periodic stress amplitude in our experiments match that of the tidal flexing we calculate the frequency shift of the experimental data. The convection stress is estimated as

$$\sigma \cong (0.1 - 0.01)\rho g \alpha_V (\Delta T) D, \tag{4}$$

where ρ is density ($\rho_{\text{icel}} = 920$ kg m^{-3}), g is gravitational acceleration, α_V is the coefficient of volumetric thermal expansion ($\alpha_{V,\text{icel}} = 1.6 \times 10^{-4}$ K^{-1}), ΔT is the magnitude of the temperature fluctuations driving convection (or, alternately the difference in temperature from the bottom to top of the convecting layer), and D is the convecting layer thickness (Barr and Showman, 2009, cf. Tobie et al., 2003, 2005; Solomatov and Moresi, 2000). For Europa, $g = 1.314$ m s^{-2}, $D = 12$ km and $\Delta T = 270$–230 K $= 40$ K

(Tobie et al., 2003). Substituting all of these values yields a convection stress of $\sigma \approx 1$ to 10 kPa and so corresponds with a subgrain size ranging from $d_{SG} = 3.7$ cm (1 kPa) to $d_{SG} = 0.37$ cm (10 kPa; Raj and Pharr, 1986). As presented earlier, our data, with $\sigma_m = 1$ MPa, has a $d_{SG} = 37$ μm. Now that we have estimated a subgrain size, the next task is to extrapolate to icy satellites using a physical approach.

Factors like temperature and grain size affect the frequency of the dynamic response (e.g., Nowick and Berry, 1972 (p. 458); Cooper, 2002): f is proportional to $(d_{SG})^p \exp(E_A/RT)$. Thus, the extrapolation for the subgrain size, holding both T and σ_0 constant, is $(f_1/f_2) = (d_{SG2}/d_{SG1})^p$. Accordingly, we extrapolate the data for 240 K (Fig. 3; $\varphi = 0.33$) to the subgrain size associated with convection at $\sigma = 1$ kPa and determine the value of Q_E at $f = 10^{-5}$ Hz, the tidal flexing frequency. For $p = 3$, the (1 kPa, 10^{-5} Hz) conditions produce $Q_E = 100$ ($Q_E^{-1} = 0.01$); for $p = 2$, one discerns $Q_E = 10$ ($Q_E^{-1} = 0.10$). This latter value is provocative, perhaps, in that $Q = 10$ was a foundational assumption in the Europan heat budget (Ojakangas and Stevenson, 1989).

We argue, however, that experimental and theoretical geophysics can and should do better than this. The change in slope of the log f v. log Q^{-1} spectrum in Fig. 3b is related to real physics. It results from the intrinsic viscosity of grain boundaries (e.g., Sundberg and Cooper, 2010; Morris and Jackson, 2009; cf. Gifkins, 1976) or, more likely in the geophysical setting, of subgrain boundaries (e.g., Cooper, 2002). As such, the extrapolated numbers for Q_E^{-1} in the previous paragraph are diminished ones, that is, we anticipate greater attenuation in polycrystalline ice at the tidal frequency of 10^{-5} Hz for an ice shell convecting under a stress of ∼1 kPa. Additionally stress concentrations in the shell, associated perhaps with features detected and characterized on the surface, become sites for additional heat input. As localized heat input affects local viscosity, mechanical instability and strain heterogeneity within the shell can be anticipated. The crucial scientific insight required to extrapolate laboratory measurements of mechanical dissipation to planetary conditions is a characterization of the materials physics behind the observed $\varphi = \varphi(f, T, \sigma_m)$ relationship and its parameterization for incorporation into models for dynamics in ice shells.

5. Conclusions

It has long been known that frequency, temperature, and pressure affect attenuation. Grain size has also been documented to greatly affect attenuation, but specifically for very fine grain sizes at conditions where the median stress is small, approaching zero. These are conditions that only infrequently conform to geologic settings. This study explored the effect of a persistent creep stress combined with small amplitude perturbations, as would be the case for a seismic wave passing through an actively deforming (tectonic) region in the Earth or for an icy shell experiencing both convective and tidal stresses. Contrary to previous low-stress studies, we find grain size to be unimportant in the attenuation response compared to the deformation-induced subgrain size. And in polycrystalline ice, additional energy dissipation comes from motion of lattice dislocations. These two effects manifest as a measured attenuation significantly higher than that predicted by a simple Maxwell solid model. Additional understanding about how the attenuation scales with median stress and accumulated strain, a focus of current studies, may elucidate the origin of anomalously high heat fluxes observed on icy satellites.

Acknowledgements

The authors thank Marc Hesse for assistance with mechanical data reduction, Sara Berglund for help in fabricating samples, Yasuko Takei for many fruitful discussions about anelasticity and scaling, the U.S.G.S. in Menlo Park, CA for use of their cryo-S.E.M., and Al Tente and Brian Corkum (both at Brown University) for their technical support with the experiments. The authors also thank H. de Bresser and a second, anonymous reviewer for thorough and helpful formal reviews of this manuscript. This research was supported financially, in part, by grants (to RFC) from the NASA Program in Planetary Geology and Geophysics (NNX06AD67G) and the NSF Program in Geophysics (EAR-1014476).

Appendix A. Details of experimental method

A.1. Sample fabrication

We used three different methods of sample preparation in order to obtain specimens with four distinct grain sizes. Coarse grain size samples (C) were created by bulk solidification. Pre-scored test tubes, 1 cm ID and 6.4 cm long, were filled with distilled water and placed upright in a polystyrene holder that included a well. Liquid nitrogen (77 K) was poured into the well while the entire holder rested within a freezer (∼253 K). Solidification of the sample proceeded from the test-tube bottom at a rate of approximately 20 μm s^{-1}. Specimens were sectioned from the middle of the test tube. The C samples fabricated with this method displayed grains with an average size of 300 ± 60 μm (Fig. 1c and Table 1 of the text proper).

The second method of sample fabrication was droplet solidification followed by hot pressing (Goldsby and Kohlstedt, 1997). Distilled water was nebulized into air by a Bernoulli-effect nozzle with orifice diameter ∼0.5 mm. The nebulization nozzle siphoned the water at a rate of ∼50 mL h^{-1} and sprayed the mist directly into a reservoir of liquid nitrogen; the droplets traversed in air a distance of ∼1 cm before entering the liquid nitrogen bath. The result was a solid/liquid nitrogen slurry that was subsequently sieved to collect ice grains of a desired size. Once the liquid nitrogen fully evaporated, this ice powder was "hot" pressed at 196 K ($T/T_m = 0.72$) and 100 MPa for 2 h in an actively evacuated (∼0.1 kPa), stainless steel cylindrical die. This sample preparation method yielded a dense cylindrical specimen with uniform grain size. M samples having a grain size ≤ 180 μm and F samples with a grain size of 19.9 ± 3.0 μm (Fig. 1b and Table 1) were prepared by this method.

The final method of sample fabrication utilized the ice-II-to-ice-I transformation in a pressure release protocol described by Durham et al. (1997, 2001), in which samples initially prepared by droplet solidification/hot-pressing, described above, were transformed to ice-II by holding them at $P = \sim 250$ MPa for 5 min. The pressure was then quickly released, which causes rapid nucleation of ice-I at the grain boundaries. After the pressure release, samples were held at 100 MPa for another two hours. Since kinetics of nucleation are fast and kinetics of crystal growth are sluggish, the VF prepared by this method exhibited small and uniform grains that were 8.4 ± 1.8 μm (Fig. 1a and Table 1).

All fabrication methods resulted in cylindrical test specimens that were approximately 10 mm in diameter. The ends of specimens were shaved smooth with a razor blade. Lengths of specimens ranged from 14 to 16 mm.

A.2. Apparatus, mechanical testing and data analysis protocol

In this study, Young's modulus and attenuation of polycrystalline ice-I were measured in compressive cyclic loading tests (Lee and Cooper, 1997) using a servomechanical-actuator testing apparatus (Model 1361 Load Frame and Model 8500 Digital Servo Control, Instron Corp.) that was modified for cold-temperature work. The apparatus, as shown schematically in Fig. A.1, has several

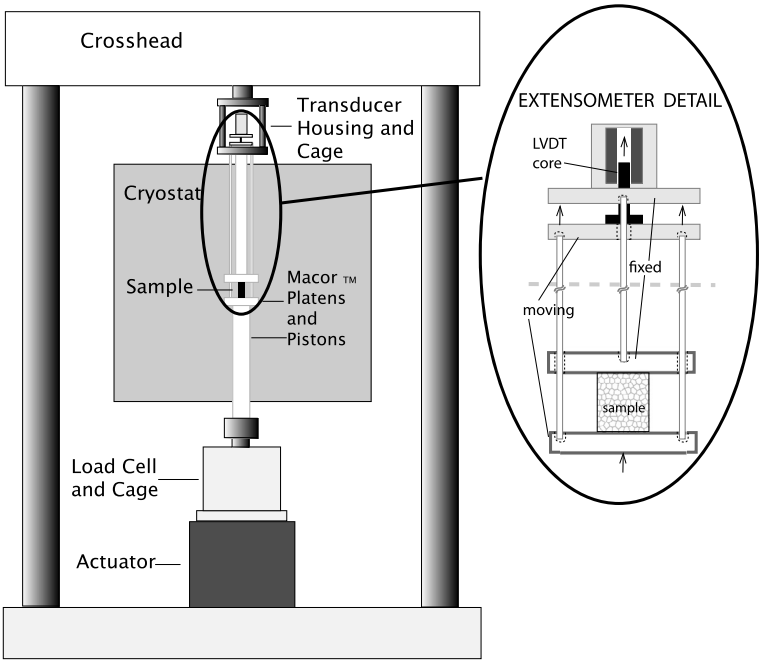

Fig. A.1. Apparatus used for compression–compression cyclic loading experiments (schematic). Three features to note are (1) the cryostat, which uses circulating nitrogen gas as the temperature regulator, (2) the free-floating, gravity-fed LVDT extensometer that sits outside the cold chamber and is accessible within an open cage, and (3) the load train made entirely of low-thermal-conductivity, high-stiffness Macor™ fluorophlogopite glass-ceramic.

custom-designed/fabricated features including a circulating air (nitrogen gas) cryostat, a gravity-fed extensometer located outside the cryostat (Fig. A.1 inset), and a fully ceramic (Macor™) load train.

A sinusoidally varying stress about a constant median differential stress was applied in load control and the resulting displacement was measured with the extensometer, which employs a linear variable differential transformer (LVDT); load, displacement and temperature data were recorded on a computer via LabView. In all cases, the cryostat and load train were brought to the desired temperature and held there for at least one hour. The sample was then placed in position without load and allowed to equilibrate for 1–2 h. The compressive median differential stress was then applied and the sample allowed to creep for 1–2 h, sufficient to achieve a nominal steady–state (as evidenced in monitoring displacement as a function of time) before the periodic loading commenced (Fig. A.2a). Approximately six cycles were run for each testing frequency, which, depending on how many frequencies were measured, totaled between 5 and 9 h of testing. Prior to and after testing, samples were stored in dry ice ($T = 195$ K). Based on the work of Goldsby and Kohlstedt (1997, 2001), we expect no microcracking to have occurred in the VF, F, or M samples. In their study, samples made via the same protocols were deformed at comparable stresses to much larger strains in both the $n = 1.8$ and $n = 2.4$ regimes using an ambient pressure apparatus. The deformed samples in this parallel study were transparent and therefore free of cavities or microcracks. Although post-deformation microscopy was performed on one C sample and no evidence of microcracking was observed, we cannot definitively rule it out in the coarse grain-sized samples.

Typical raw experimental data are shown in Fig. A.2b, in which time has been zeroed arbitrarily. The monotonic downward trend of the displacement data is a result of steady–state creep associated with the applied median differential stress, $\sigma_m = 1$ MPa. Sinusoids were fitted to the collected data using a Levenberg–Marquardt algorithm, seeking parameters consistent with 95% confidence intervals. The Young's modulus and the phase difference between the applied load and the linear displacement were calculated from the phase and amplitude parameters of the fitted curves.

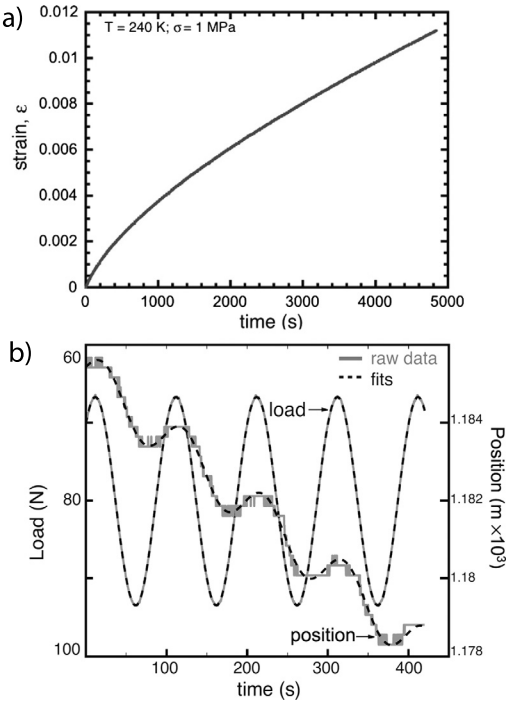

Fig. A.2. (a) Typical creep curve obtained after initial loading of sample ($\sigma_m = 1$ MPa), prior to cyclic loading. (b) Typical raw data for Q_E^{-1} experiments (gray). A numerical algorithm fits curves (black dashed line) to both the load and displacement data and so provides an output with the phase difference. The approach isolates the mechanical testing frequency from other, higher-frequency noise associated with, e.g., temperature fluctuation. For both figures, the data shown were collected while testing very fine grain sized samples (VF) at $T = 240$ K. For (b), $f = 0.01$ Hz, the applied median stress was $\sigma_m = 1$ MPa, and the periodic stress amplitude was $\sigma_0 = 0.16$ MPa.

The error in experimental determination of attenuation in subresonant tests like the ones pursued here is primarily in measuring the phase lag δ separating the applied stress and achieved strain ($Q^{-1} = \tan\delta$). Other sources of error such as strain resolution of the LVDT and temperature fluctuation are not expected to be significant compared with the error in measuring δ. For these experiments, the error in measuring δ was determined using both the confidence intervals established by the algorithm and by performing multiple tests (three-to-five, depending on the frequency).

Our interest is in characterizing "intrinsic" attenuation, that is, the mechanical loss of a volume of material that is uniformly distorted. As long as the material responds as linear viscoelastic, meaning that the attenuation is not a function of strain amplitude, then the attenuation measured in the experiments is identical to the intrinsic attenuation. As indicated in the Experimental Results section of the text proper, however, and as detailed below, the viscoelastic response of our ice specimens was modestly non-linear. As a consequence, we pursued a theoretical analysis to discern a correction factor between the attenuation we measured and that which is intrinsic (documented in McCarthy, 2009). We determined that the correction—corresponding to our testing geometry and to the modest degree of characterized nonlinearity—is quite small, ~6%, which is barely larger than the size of symbols on our attenuation figures and, too, well within experimental error. For this reason, we report in the text proper (and here) the attenuation values directly measured in the experiments.

Appendix B. Non-linearity of viscoelastic response

The attenuation response revealed a very modest nonlinearity—$Q_E^{-1} \propto \varepsilon_0^{0.39}$ for the range of cyclic strain amplitude explored (Fig. 2). In the absence of cracking, which is the case in our experiments, non-linear response is associated with the presence and motion of lattice dislocations (e.g., Karato and Spetzler, 1990; Nowick and Berry, 1972 [Ch. 11]), although, as explained in the text proper, most experimental and theoretical characterizations of dislocation-effected attenuation in crystalline materials have emphasized conditions at distinctly higher frequencies and lower homologous temperatures than are active in Earth/planetary situations, particularly for water ice.

An exception is the work of Tatibouet et al. (1986, 1987) who studied low-frequency attenuation in ice single crystals, engineered bicrystals and polycrystalline aggregates. For experiments on single crystals (described as "undeformed") and using frequencies in the range $10^{-3} \le f(\text{Hz}) \le 1$ and strain amplitudes in the range $2 \times 10^{-5} \le \Delta\varepsilon_0 \le 7.5 \times 10^{-5}$, the authors identified behavior similar to that described here: modest non-linearity where attenuation was proportional to ε_0^q where at 10^{-2} Hz q ranged from ~0.1 at 250 K to ~0.2 at 270 K. For isothermal conditions, however, the non-linearity exponent q increased significantly as the frequency was lowered. Non-linearity was not addressed explicitly in the bicrystal or polycrystalline experiments. Nevertheless, plastically deforming the bicrystals before testing their attenuation response demonstrated the same behavior of modestly nonlinear response that was, too, frequency dependent. While the authors characterized the behavior predicated on dislocation climb and glide dynamics—either of lattice dislocation in the single crystals or of intrinsic grain boundary dislocations in the case of bicrystals and polycrystals—the sensitivity of the high-temperature background characterized in their experiments is at least equally well considered by the combination of chemical diffusion and dislocation emission and glide that we articulate in the text proper.

Appendix C. The Andrade model

In Fig. 5 of the text, the gray line behind the master curve experimental data is a frequency-transformation of the Andrade solid model, which incorporates elastic, anelastic and plastic responses (Andrade, 1910):

$$J(t) = \frac{\varepsilon(t)}{\sigma} = J_U + \beta t^{\psi} + \frac{t}{\eta_{ss}} \tag{C.1}$$

where J_U is the unrelaxed compliance, β is a constant ($\beta \ll 1$), t is time, ψ ranges from 1/4 to 1/2 and η_{ss} is the steady–state viscosity. The Andrade model was first applied to ice by Duval (1976, 1978). The storage and loss components of the Andrade model's complex compliance take the forms:

$$J_1(\omega) = J_U + \beta\Gamma(1+\psi)\omega^{-\psi}\cos\left(\frac{\psi\pi}{2}\right) \quad \text{and} \tag{C.2}$$

$$J_2(\omega) = \beta\Gamma(1+\psi)\omega^{-\psi}\sin\left(\frac{\psi\pi}{2}\right) + \frac{1}{\eta_{ss}\omega}, \tag{C.3}$$

respectively, where ω is angular frequency ($\equiv 2\pi f$) and Γ is the gamma function. The Andrade model shown in Fig. 5 is normalized by the Maxwell frequency using an estimated viscosity for grain boundary diffusion creep in ice (1.4×10^{16} Pa s; Goldsby and Kohlstedt, 2001) and the best-fit parameters for β and ψ (4.5×10^{-12} and 0.25, respectively). As the figures show, the shape of the high temperature background, attributed to the diffusion accommodated grain-boundary relaxation mechanism, is generally well captured by the Andrade function. Data generally deviate from the Andrade model at high-normalized frequency where it is considered that another mechanism is dominating the anelastic response (Sundberg and Cooper, 2010; Jackson et al., 2014; Takei et al., 2014).

References

Andrade, E.N.D., 1910. On the viscous flow in metals, and allied phenomena. Proc. R. Soc. Lond. A 84, 1–12.

Barr, A.C., Showman, A.P., 2009. Heat transfer in Europa's icy shell. In: Pappalardo, R.T., McKinnon, W.B., Khurana, K. (Eds.), Europa. University of Arizona Press, Tucson, AZ, pp. 405–430.

Berckhemer, H., Kampfmann, W., Aulbach, E., Schmeling, H., 1982. Shear modulus and Q of forsterite and dunite near partial melting from forced-oscillation experiments. Phys. Earth Planet. Inter. 29, 30–41.

Chiang, S-W., Kohlstedt, D.L., 1985. Load relaxation studies of germanium. J. Mater. Sci. 20 (2), 736–755.

Coble, R.L., 1963. A model for boundary diffusion controlled creep in polycrystalline materials. J. Appl. Phys. 34, 1679–1682.

Cole, D.M., Durell, G.D., 2001. A dislocation-based analysis of strain history effects in ice. Philos. Mag. A 81, 1849–1872.

Cooper, R.F., 2002. Seismic wave attenuation: energy dissipation in viscoelastic crystalline solids. Rev. Mineral. Geochem. 51, 253–290.

Crossman, F.W., Ashby, M.F., 1975. The non-uniform flow of polycrystals by grain boundary sliding accommodated by power-law creep. Acta Metall. 23, 425–440.

Cullen, D., Baker, I., 2001. Observations of impurities in ice. Microsc. Res. Tech. 55, 198–207.

Durham, W.B., Kirby, S.H., Stern, L.A., 1997. Creep of water ices at planetary conditions: a compilation. J. Geophys. Res. 102, 16293–16302.

Durham, W.B., Stern, L.A., Kirby, S.H., 2001. Rheology of ice I at low stress and elevated confining pressure. J. Geophys. Res. 106 (6), 11031–11042.

Duval, P., 1976. Temporary or permanent creep laws of polycrystalline ice for different stress conditions. Ann. Geophys. 32, 335–350.

Duval, P., 1978. Anelastic behaviour of polycrystalline ice. J. Glaciol. 21 (85), 621–628.

Farla, R.J.M., Jackson, I., Fitz Gerald, J.D., Faul, U.H., Zimmerman, M.E., 2012. Dislocation damping and anisotropic seismic wave attenuation in Earth's upper mantle. Science 336, 332–335.

Frost, H.J., Ashby, M.F., 1982. Deformation-Mechanism Maps: The Plasticity and Creep of Metals and Ceramics. Pergamon Press, Oxford, UK, p. 166.

Gammon, P.H., Kiefte, H., Clouter, M.J., Denner, W.W., 1983. Elastic constants of ar-

tificial and natural ice samples by Brillouin spectroscopy. J. Glaciol. 29 (103), 433–460.
Gifkins, R.C., 1970. Optical Microscopy of Metals. Elsevier, New York, p. 208.
Gifkins, R.C., 1976. Grain-boundary sliding and its accommodation during creep and superplasticity. Metall. Trans. A 7A, 1225–1232.
Goldsby, D.L., Kohlstedt, D.L., 1997. Grain boundary sliding in fine-grained ice I. Scr. Mater. 37, 1399–1406.
Goldsby, D.L., Kohlstedt, D.L., 2001. Superplastic deformation of ice: experimental observations. J. Geophys. Res. 106 (B6), 11017–11030.
Granato, A., Lücke, K., 1956a. Application of dislocation theory to internal friction phenomena at high frequencies. J. Appl. Phys. 27 (7), 789–805.
Granato, A., Lücke, K., 1956b. Theory of mechanical damping due to dislocations. J. Appl. Phys. 27, 583–593.
Greenberg, R., et al., 1998. Tectonic processes on Europa: tidal stresses, mechanical response and visible features. Icarus 135, 64–78.
Gribb, T.T., Cooper, R.F., 1998. Low-frequency shear attenuation in polycrystalline olivine: grain boundary diffusion and the physical significance of the Andrade model for viscoelastic rheology. J. Geophys. Res. 103, 27267–27279.
Gueguen, Y., Darot, M., Mazot, P., Woirgard, J., 1989. Q^{-1} of forsterite single crystals. Phys. Earth Planet. Inter. 55, 254–258.
Hamann, I., Weikusat, C., Azuma, N., Kipfstuhl, S., 2007. Evolution of ice crystal microstructure during creep experiments. J. Glaciol. 53, 479–489.
Hart, E.W., 1970. A phenomenological theory for plastic deformation of polycrystalline metals. Acta Metall. 21, 295–307.
Hart, E.W., Solomon, H.D., 1973. Load relaxation studies of polycrystalline high-purity aluminum. Acta Metall. 21 (3), 295–307.
Hiraga, T., Miyazaki, T., Tasaka, M., Yoshida, H., 2010. Mantle superplasticity and its self-made demise. Nature 468, 1091–1094.
Jackson, I., Faul, U.H., Skelton, R., 2014. Elastically accommodated grain-boundary sliding: new insights from experiment and modeling. Phys. Earth Planet. Inter. 228, 203–210.
Jackson, I., FitzGerald, J.D., Faul, U.F., Tan, B.H., 2002. Grain-size-sensitive seismic-wave attenuation in polycrystalline olivine. J. Geophys. Res. 107 (B12), 2360. http://dx.doi.org/10.1029/2001JB001225.
Karato, S-i., Spetzler, H.A., 1990. Defect microdynamics in minerals and solid-state mechanisms of seismic wave attenuation and velocity dispersion in the mantle. Rev. Geophys. 28, 399–421.
Lakes, R.S., 1999. Viscoelastic Solids. CRC Press, Boca Raton, FL, p. 476.
Lee, J.A., Cooper, R.F., 1997. Internal friction/attenuation in a beta-spodumene glass-ceramic. J. Am. Ceram. Soc. 80, 2917–2928.
Lerner, I., Chiang, S-W., Kohlstedt, D.L., 1979. Load relaxation studies of four alkali halides. Acta Metall. 27, 1187–1196.
Lubarda, V.A., Blume, J.A., Needleman, A., 1993. An analysis of equilibrium dislocation distributions. Acta Metall. Mater. 41, 625–642.
McCarthy, C., 2009. The microstructures and creep and attenuation behaviors of ice-I and ice/hydrate eutectic aggregates at planetary conditions. Ph.D. Dissertation. Brown University, Providence, RI.
McCarthy, C., Cooper, R.F., Kirby, S.H., Rieck, K.D., Stern, L.A., 2007. Solidification and microstructures of binary ice-I/hydrate eutectic aggregates. Am. Mineral. 92, 1550–1560.
McCarthy, C., Takei, Y., Hiraga, T., 2011. Experimental study of attenuation and dispersion over a broad frequency range: 2. The universal scaling of polycrystalline materials. J. Geophys. Res. 116, B09207.
Miguel, M., Vespignani, A., Zapperi, S., Weiss, J., Grasso, J., 2001. Intermittent dislocation flow in viscoplastic deformation. Nature 410 (6829), 667–671.
Minster, J.B., Anderson, D.L., 1981. A model of dislocation-controlled rheology for the mantle. Philos. Trans. R. Soc. Lond. A 299, 319–356.
Morris, S.J.S., Jackson, I., 2009. Implications of the similarity principle relating creep and attenuation in finely grained solids. Mater. Sci. Eng. A 521–522, 124–127.
Nowick, A.S., Berry, B.S., 1972. Anelastic Relaxation in Crystalline Solids. Academic Press, San Diego, CA, p. 677.
Ojakangas, G.W., Stevenson, D.J., 1989. Thermal state of an ice shell on Europa. Icarus 81 (2), 220–241.
Pappalardo, R.T., et al., 1998. Geological evidence for solid-state convection in Europa's ice shell. Nature 391, 365–367.
Puthoff, J., 2005. Mesoscale modeling of dislocation bursts during high-temperature plastic deformation. MSc Thesis. University of Wisconsin–Madison, Madison, WI.
Raj, R., 1975. Transient behavior of diffusion-induced creep and creep rupture. Metall. Trans. A 6A, 1499–1590.
Raj, R., Ashby, M.F., 1971. On grain boundary sliding and diffusional creep. Metall. Trans. 2, 1113–1127.
Raj, S.V., Pharr, G.M., 1986. A compilation and analysis of data for the stress dependence of the subgrain size. Mater. Sci. Eng. 81 (1–2), 217–237.
Richeton, T., Weiss, J., Louchet, F., 2005. Breakdown of avalanche critical behaviour in polycrystalline plasticity. Nat. Mater. 4 (6), 465–469.
Shoji, D., Hussman, H., Kurita, K., Sohl, F., 2013. Ice rheology and the tidal heating of Enceladus. Icarus 226, 10–19.
Solomatov, V.S., Moresi, L.N., 2000. Scaling of time-dependent stagnant lid convection: application to small-scale convection on earth and other terrestrial planets. J. Geophys. Res. 105 (B9), 21795–21817.
Stone, D.S., 1991. Scaling laws in dislocation creep. Acta Metall. Mater. 39 (4), 599–608.
Stone, D.S., Plookphol, T., Cooper, R.F., 2004. Similarity and scaling in creep and load relaxation of single-crystal halite (NaCl). J. Geophys. Res. 109, B12201. http://dx.doi.org/10.1029/2004JB003064.
Sundberg, M., Cooper, R.F., 2010. A composite viscoelastic model for incorporating grain boundary sliding and transient diffusion creep; correlating creep and attenuation responses for materials with a fine grain size. Philos. Mag. 90, 2817–2840.
Sutton, A.P., Balluffi, R.W., 1995. Interfaces in Crystalline Materials. Clarendon Press-Oxford, Oxford, United Kingdom, p. 819.
Takei, Y., Karasawa, F., Yamauchi, H., 2014. Temperature, grain size, and chemical controls on polycrystal anelasticity over a broad frequency range extending into the seismic range. J. Geophys. Res. 119 (7), 5414–5443.
Tan, B.H., Jackson, I., Fitz Gerald, J.D., 2001. High-temperature viscoelasticity of fine-grained polycrystalline olivine. Phys. Chem. Miner. 28 (9), 641–664.
Tatibouet, J., Perez, J., Vassoille, R., 1986. High-temperature internal friction and dislocations in ice Ih. J. Phys. 47, 51–60.
Tatibouet, J., Perez, J., Vassoille, R., 1987. Study of grain boundaries in ice by internal friction measurement. J. Phys. 48, 197–203.
Thompson, E., Dillman, A.M., Hansen, L.N., Kohlstedt, D.L., 2011. Contribution of grain boundary sliding to diffusion creep of forsterite. Abstract #T52B-03, Presented at the American Geophysical Union Fall Meeting, San Francisco, CA, 9 December 2011.
Tobie, G., Choblet, G., Sotin, C., 2003. Tidally heated convection: constraints on Europa's ice shell thickness. J. Geophys. Res. 108 (E11), 5124. http://dx.doi.org/10.1029/2003JE002099.
Tobie, G., Mocquet, A., Sotin, C., 2005. Tidal dissipation within large icy satellites: applications to Europa and Titan. Icarus 177, 534–549.
Twiss, R.J., 1977. Theory and applicability of a recrystallized grain size paleopiezometer. Pure Appl. Geophys. 115, 227–244.
Weathers, M.S., Bird, J.M., Cooper, R.F., Kohlstedt, D.L., 1979. Differential stress determined from deformation-induced microstructures of the Moine Thrust Zone. J. Geophys. Res. 84, 7495–7509.
Weertman, J., Weertman, J.R., 1983. Mechanical properties, strongly temperature-dependent. In: Cahn, J.W., Haasen, P. (Eds.), Physical Metallurgy, third edition. Elsevier Science Publishers B.V., Amsterdam, pp. 1309–1340.
Weikusat, I., Kipfstuhl, S., Faria, S.H., Azuma, N., Miyamoto, A., 2009. Subgrain boundaries and related microstructural features in EDML (Antarctica) deep ice core. J. Glaciol. 55, 461–472.
Weiss, J., Ben Rhouma, W., Richeton, T., Dechanel, S., Louchet, F., Truskinovsky, L., 2015. From mild to wild fluctuations in crystal plasticity. Phys. Rev. Lett. 114, 105504.
Zaiser, M., Hähner, P., 1999. The flow stress of fractal dislocation arrangements. Mater. Sci. Eng. A 270 (2), 299–307.